PHYSICAL REVIEW D **87,** 016004 (2013)

Analysis of $\mu - \tau$ conversion through $\mu N \to \tau X$ deep inelastic scattering induced by unparticles

A. Bolaños, A. Fernandez, A. Moyotl, and G. Tavares-Velasco*

Facultad de Ciencias Físico Matemáticas, Benemérita Universidad Autónoma de Puebla, Apartado Postal 1152, Puebla Puebla, México

(Received 6 October 2012; published 4 January 2013)

A study of $\mu - \tau$ conversion via the deep inelastic scattering process $\mu N \to \tau X$, with N a nucleon, is performed taking into account the effects from both spin-0 and spin-1 unparticles with lepton flavor violating (LFV) couplings. This process has attracted attention in the past as it may be at the reach of a future neutrino or muon factory. For the model parameters, we use the most recent constraints on the unparticle LFV couplings from the experimental limits on the muon anomalous magnetic moment and the LFV decay $\tau \to 3\mu$, whereas for the unparticle scale $\Lambda_{\mathcal{U}}$ and scale dimension $d_{\mathcal{U}}$, we use the bounds obtained from the search for monojets plus missing transverse energy at the LHC. The $\mu N \to \tau X$ cross section is analyzed when the target is a proton, and it is found that the unparticle effects can be larger than the contribution from Higgs exchange in the minimal supersymmetric standard model. We also analyze the behavior of the angular and energy distributions of the emitted tau lepton, which could be used to disentangle among distinct new physics contributions. It is found that, for a beam with an intensity of 10^{20} muons with an energy around 50 GeV on a 10^2 gr/cm^2 mass target annually, there would be about 10^2–10^3 $\mu N \to \tau X$ events per year. The potential background is discussed briefly.

DOI: 10.1103/PhysRevD.87.016004 PACS numbers: 11.30.Hv, 13.85.Fb, 13.85.Qk

I. INTRODUCTION

Georgi has conjectured a hidden scale invariant sector in the high-energy theory [1,2] that could interact with the standard model (SM) via scale invariant fields associated with the so-called unparticles, a denomination due to the fact that scale invariant fields with nontrivial anomalous dimension cannot be interpreted in terms of particles. Although the description of such a theory could be extremely complex, one can still study its low-energy effects through the effective Lagrangian approach. The ingredients to describe the effective Lagrangian that parametrizes the unparticle interactions with the SM can be found in Ref. [3]: the hidden sector is a Banks and Zaks ($\mathcal{BZ}$) sector, and the associated fields are introduced through renormalizable operators $\mathcal{O}_{\mathcal{BZ}}$. The interaction of this sector with the SM fields occurs through the exchange of heavy particles at a very high-energy scale $M_{\mathcal{U}}$. Below such a scale, there emerge nonrenormalizable couplings between the $\mathcal{BZ}$ sector and the SM. As scale invariance emerges, dimensional transmutation proceeds via the renormalizable couplings of the $\mathcal{BZ}$ sector at an energy scale $\Lambda_{\mathcal{U}}$. An effective theory can describe the interactions of the $\mathcal{BZ}$ and SM fields, which occur via unparticles. The effective Lagrangian can be written as [1,2]

$$\mathcal{L}_{\mathcal{U}} = C_{\mathcal{O}_{\mathcal{U}}} \frac{\Lambda_{\mathcal{U}}^{d_{\mathcal{BZ}}-d_{\mathcal{U}}}}{M_{\mathcal{U}}^{d_{\mathrm{SM}}+d_{\mathcal{BZ}}-4}} \mathcal{O}_{\mathrm{SM}} \mathcal{O}_{\mathcal{U}}, \tag{1}$$

where $C_{\mathcal{O}_{\mathcal{U}}}$ stands for the coupling constant, whereas the unparticle operator, $\mathcal{O}_{\mathcal{U}}$, can be of fractional dimension $d_{\mathcal{U}}$. The unparticle operators, which can be constructed out of the primary operators $\mathcal{O}_{\mathcal{BZ}}$ and their transmutation, can be of scalar, vector, spinor, or tensor type. Unparticle propagators are constructed using unitary cuts and the spectral decomposition formula. By this means, the propagator of a spin-0 unparticle is found to be

$$\Delta_F(p^2) = \frac{A_{d_{\mathcal{U}}}}{2\sin(d_{\mathcal{U}}\pi)}(-p^2 - i\epsilon)^{d_{\mathcal{U}}-2}, \tag{2}$$

where the $A_{d_{\mathcal{U}}}$ function is introduced to normalize the spectral density [4] and is given as follows:

$$A_{d_{\mathcal{U}}} = \frac{16\pi^2\sqrt{\pi}}{(2\pi)^{2d_{\mathcal{U}}}} \frac{\Gamma(d_{\mathcal{U}} + \frac{1}{2})}{\Gamma(d_{\mathcal{U}} - 1)\Gamma(2d_{\mathcal{U}})}. \tag{3}$$

As for the propagator of a spin-1 unparticle, it is

$$\Delta_F^{\mu\nu}(p^2) = \Delta_F(p^2)\left(-g^{\mu\nu} + a\frac{p^\mu p^\nu}{p^2}\right). \tag{4}$$

The condition $a = 1$ is fulfilled when the unparticle field is transverse, namely, $p_\mu \Delta_F^{\mu\nu}(p^2) = 0$.

Unparticle phenomenology has been widely studied. For instance, peculiar effects arising from the interference between unparticle and SM contributions could show up in the Drell-Yan process at hadronic colliders [5–7]. The direct production of unparticles has also been studied in both leptonic [4] and hadronic colliders [8]. Not only the tree-level unparticle effects have been the focus of attention, but also one-loop induced effects [9–13]; the electron magnetic dipole moment via scalar and vector unparticles was first obtained in Refs. [14,15]. This study was later extended for the lepton magnetic moment due to scalar [9] and vector [11] unparticles with lepton flavor

*gtv@fcfm.buap.mx

violating (LFV) couplings, whereas the lepton electric dipole moment via scalar [10] and vector [11] unparticles was studied more recently. Other studies worth mentioning deal with the potential unparticle effects on CP violation [16,17], neutrino physics [18], etc. Direct constraints on the scale $\Lambda_{\mathcal{U}}$ and the dimension $d_{\mathcal{U}}$ have been extracted from the LEP, Tevatron, and LHC data. For instance, the $e^- e^+ \to \gamma \mathcal{U}$ process was studied to explain $\gamma \bar{\nu} \nu$ production at the LEP [4]. More recently, the CMS collaboration has imposed constraints on the unparticle parameters from the data of the search for monojets plus large missing transverse energy at the LHC [19]. Indirect constraints have also been obtained from experimental data in cosmology, astrophysics [20–23], the muon magnetic dipole moment (MDM), and LFV processes [9,11].

As far as LFV is concerned, it is well known that any signal of this class of transitions would be a clear evidence of new physics. Strong experimental constraints on LFV muon decays have been placed that considerably disfavor this class of processes: $\mathrm{BR}(\mu \to e\gamma) < 2.4 \times 10^{-12}$ [24], $\mathrm{BR}(\mu \to 3e) < 1.0 \times 10^{-12}$ [25], and $\mathrm{BR}(\mu \mathrm{Ti} \to e \mathrm{Ti}) < 3.6 \times 10^{-11}$ [26]. On the other hand, there are less stringent constraints on LFV tau decays: $\mathrm{BR}(\tau \to e\gamma) \lesssim 10^{-8}$, $\mathrm{BR}(\tau \to \mu\gamma) \lesssim 10^{-8}$ [27], $\mathrm{BR}(\tau \to 3e) < 3.6 \times 10^{-8}$ [28], and $\mathrm{BR}(\tau \to e^- e^+ \mu) < 3.7 \times 10^{-8}$ [29]. Therefore, there is still a chance that $\mu - \tau$ transitions may occur with a measurable rate. Such a possibility has been explored in several SM extensions. In this work we are interested in the study of $\mu - \tau$ conversion via the deep inelastic scattering (DIS) process $\mu N \to \tau X$, where N is a nucleon, in the context of unparticle physics. This process, which could be at the reach of a future neutrino or muon factory, has attracted some attention during the past [30–32]. We will consider the contributions from both spin-0 and spin-1 unparticles assuming the current bounds on the unparticle scale and the LFV unparticle couplings. The tensor unparticle contribution will not be considered as it is suppressed by the inverse of $\Lambda_{\mathcal{U}}^2$, which stems from the fact that the spin-2 unparticle operator is of higher dimension than that of the spin-0 and spin-1 unparticles. The study of $\mu - \tau$ conversion induced by LFV scalar- and vector-mediated, four fermion couplings, $\bar{\tau} \mu \bar{q} q$, via DIS has already been discussed in the context of effective Lagrangians [31] and the minimal supersymmetric standard model (MSSM) [32]. It was concluded that a 50 GeV muon beam with intensity of 10^{20} muons on a nucleon target per year, as expected in a neutrino factory [33], would allow for about 10^6–10^7 $\mu N \to \tau X$ events annually as long as the corresponding cross section is of the order of a few fb. This rate could give some room for either detecting the signal or placing stringent limits on $\mu - \tau$ couplings.

The rest of the work is organized as follows. Section II is devoted to the calculation of the process $\mu N \to \tau X$ in the context of unparticle physics. The numerical analysis and discussion is presented in Sec. III. Finally, the conclusions and outlook are presented in Sec. IV.

II. $\mu N \to \tau X$ CROSS SECTION FROM UNPARTICLE INTERACTIONS

We will consider the DIS process $\mu N \to \tau X$ due to lepton flavor violating unparticle interactions, which arises through the Feynman diagram of Fig. 1. We are neglecting flavor changing transitions in the quark sector. The most general renormalizable effective operators for the couplings of spin-0 and spin-1 unparticles to a fermion pair are [1]

$$\mathcal{L}_{\mathcal{U}^0} = \frac{\lambda_S^{ij}}{\Lambda_{\mathcal{U}}^{d_{\mathcal{U}}-1}} \bar{f}_i f_j \mathcal{O}_{\mathcal{U}^0} + \frac{\lambda_P^{ij}}{\Lambda_{\mathcal{U}}^{d_{\mathcal{U}}-1}} \bar{f}_i \gamma^5 f_j \mathcal{O}_{\mathcal{U}^0}, \tag{5}$$

$$\mathcal{L}_{\mathcal{U}^1} = \frac{\lambda_V^{ij}}{\Lambda_{\mathcal{U}}^{d_{\mathcal{U}}-1}} \bar{f}_i \gamma_\mu f_j \mathcal{O}^\mu_{\mathcal{U}^1} + \frac{\lambda_A^{ij}}{\Lambda_{\mathcal{U}}^{d_{\mathcal{U}}-1}} \bar{f}_i \gamma_\mu \gamma^5 f_j \mathcal{O}^\mu_{\mathcal{U}^1}, \tag{6}$$

where i and j are flavor indexes. For the flavor diagonal couplings we will adopt the notation $\lambda_J^{ii} \equiv \lambda_J^i$, with $J = S$, P, A, and V.

We will neglect all the fermion masses and calculate the unpolarized double differential cross section for the constituent parton subprocesses in terms of the usual x and y variables, where $x = Q^2/(2m_N \nu)$ is the fractional longitudinal momentum carried by the struck parton and $y = \nu/E_\mu$ is the fractional energy transfer. Here Q^2 is the squared momentum transfer and $\nu = E_\mu - E_\tau$, with E_μ and E_τ the muon and tau energies in the nucleon rest frame. In terms of the Mandelstam variables of the parton subprocess, we have $Q^2 = -\hat{t} \simeq y\hat{s} = xys$, with $s = 2m_N E_\mu$ the square of the center-of-mass energy of the muon-nucleon collision. For completeness, we first write the most general expressions for the contributions of the spin-0 and spin-1 unparticles to the unpolarized double differential cross section for the subprocesses $\mu q \to \tau q$ and $\mu \bar{q} \to \tau \bar{q}$. For the spin-0 unparticle contribution we obtain

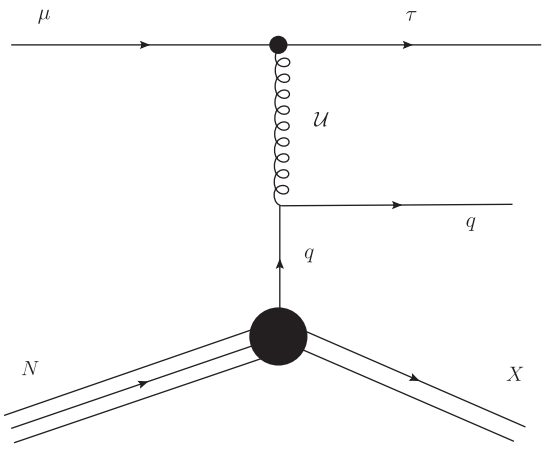

FIG. 1. Feynman diagram for $\mu N \to \tau X$ scattering due to LFV unparticle couplings. We neglect flavor change in the quark sector.

$$\frac{d^2\sigma_{\mathcal{U}^0}}{dxdy}(\mu q \to \tau q) = \frac{\hat{s}|\Delta_F(-Q^2)|^2}{16\pi\Lambda_{\mathcal{U}}^{4(d_{\mathcal{U}}-1)}}(|L^{\mu\tau}_{\mathcal{U}^0}|^2 + |R^{\mu\tau}_{\mathcal{U}^0}|^2)(|L^{q}_{\mathcal{U}^0}|^2 + |R^{q}_{\mathcal{U}^0}|^2)y^2, \tag{7}$$

which is also valid for the $\mu\bar{q} \to \tau\bar{q}$ subprocess. We have adopted the following shorthand notation for the unparticle couplings: $L^{ij}_{\mathcal{U}^0} = \lambda^{ij}_S - \lambda^{ij}_P$ and $R^{ij}_{\mathcal{U}^0} = \lambda^{ij}_S + \lambda^{ij}_P$, whereas $\Delta_F(p^2)$ is given in Eq. (2).

On the other hand, the corresponding contributions of a spin-1 unparticle are given by

$$\frac{d^2\sigma_{\mathcal{U}^1}}{dxdy}(\mu q \to \tau q) = \frac{\hat{s}|\Delta_F(-Q^2)|^2}{64\pi\Lambda_{\mathcal{U}}^{4(d_{\mathcal{U}}-1)}}(|L^{q}_{\mathcal{U}^1}|^2(|L^{\mu\tau}_{\mathcal{U}^1}|^2 + |R^{\mu\tau}_{\mathcal{U}^1}|^2(1-y)^2) + |R^{q}_{\mathcal{U}^1}|^2(|R^{\mu\tau}_{\mathcal{U}^1}|^2 + |L^{\mu\tau}_{\mathcal{U}^1}|^2(1-y)^2)), \tag{8}$$

and

$$\frac{d^2\sigma_{\mathcal{U}^1}}{dxdy}(\mu \bar{q} \to \tau \bar{q}) = \frac{\hat{s}|\Delta_F(-Q^2)|^2}{16\pi\Lambda_{\mathcal{U}}^{4(d_{\mathcal{U}}-1)}}(|L^{q}_{\mathcal{U}^1}|^2(|R^{\mu\tau}_{\mathcal{U}^1}|^2 + |L^{\mu\tau}_{\mathcal{U}^1}|^2(1-y)^2) + |R^{q}_{\mathcal{U}^1}|^2(|L^{\mu\tau}_{\mathcal{U}^1}|^2 + |R^{\mu\tau}_{\mathcal{U}^1}|^2(1-y)^2)). \tag{9}$$

with $L^{ij}_{\mathcal{U}^1} = \lambda^{ij}_V - \lambda^{ij}_A$ and $R^{ij}_{\mathcal{U}^1} = \lambda^{ij}_V + \lambda^{ij}_A$.

We can now fold the above expressions with the nucleon parton distribution functions to obtain the cross section for the process $\mu N \to \tau X$. For instance, if we consider an isoscalar nucleon $N = (n+p)/2$, with mass $m_N = (m_n + m_p)/2$, we obtain for the contribution of a spin-0 unparticle

$$\frac{d^2\sigma_{\mathcal{U}^0}}{dxdy}(\mu N \to \tau X) = \frac{m_N E_\mu}{32\pi\Lambda_{\mathcal{U}}^{4(d_{\mathcal{U}}-1)}}|\Delta_F(-Q^2)|^2 x(q_{\mathcal{U}^0}(x,Q^2) + \bar{q}_{\mathcal{U}^0}(x,Q^2))y^2, \tag{10}$$

and for the contribution of a spin-1 unparticle

$$\frac{d^2\sigma_{\mathcal{U}^1}}{dxdy}(\mu N \to \tau X) = \frac{m_N E_\mu}{8\pi\Lambda_{\mathcal{U}}^{4(d_{\mathcal{U}}-1)}}|\Delta_F(-Q^2)|^2 x(q_{\mathcal{U}^1}(x,Q^2) + \bar{q}_{\mathcal{U}^1}(x,Q^2)(1-y)^2), \tag{11}$$

where

$$q_{\mathcal{U}^0}(x,Q^2) = \bar{q}_{\mathcal{U}^0}(x,Q^2) = (|L^{\mu\tau}_{\mathcal{U}^0}|^2 + |R^{\mu\tau}_{\mathcal{U}^0}|^2)(|L^{q}_{\mathcal{U}^0}|^2 + |R^{q}_{\mathcal{U}^0}|^2) \times \left(\frac{u_v + d_v}{2} + S\right), \tag{12}$$

$$q_{\mathcal{U}^1}(x,Q^2) = (|L^{\mu\tau}_{\mathcal{U}^1}|^2|L^{q}_{\mathcal{U}^1}|^2 + |R^{\mu\tau}_{\mathcal{U}^1}|^2|R^{q}_{\mathcal{U}^1}|^2)(u_v + d_v) + (|L^{\mu\tau}_{\mathcal{U}^1}|^2 + |R^{\mu\tau}_{\mathcal{U}^1}|^2)(|L^{q}_{\mathcal{U}^1}|^2 + |R^{q}_{\mathcal{U}^1}|^2)S, \tag{13}$$

and

$$\bar{q}_{\mathcal{U}^1}(x,Q^2) = (|L^{\mu\tau}_{\mathcal{U}^1}|^2|R^{q}_{\mathcal{U}^1}|^2 + |R^{\mu\tau}_{\mathcal{U}^1}|^2|L^{q}_{\mathcal{U}^1}|^2)(u_v + d_v) + (|L^{\mu\tau}_{\mathcal{U}^1}|^2 + |R^{\mu\tau}_{\mathcal{U}^1}|^2)(|L^{q}_{\mathcal{U}^1}|^2 + |R^{q}_{\mathcal{U}^1}|^2)\bar{S}. \tag{14}$$

We have considered that the unparticle couplings to quark-antiquark pairs are flavor blind: $L^{u}_{\mathcal{U}^{0,1}} = L^{d}_{\mathcal{U}^{0,1}} = L^{q}_{\mathcal{U}^{0,1}}$, $R^{u}_{\mathcal{U}^{0,1}} = R^{d}_{\mathcal{U}^{0,1}} = R^{q}_{\mathcal{U}^{0,1}}$. Also, u_v and d_v stand for the valence quark distribution functions, whereas $S = \bar{S} = u_s + d_s + c_s + b_s + t_s$ stands for the sea quark distribution function. We omitted the explicit dependence on x and Q^2.

Unfortunately, there is dependence on several free parameters. So, without losing generality we will assume that the pseudoscalar and vector-axial unparticle couplings are negligible as compared to the scalar and vector couplings, i.e., $L^{ij}_{\mathcal{U}^0} \simeq R^{ij}_{\mathcal{U}^0} \simeq \lambda^{ij}_S$ and $L^{ij}_{\mathcal{U}^1} \simeq R^{ij}_{\mathcal{U}^1} \simeq \lambda^{ij}_V$. In fact, as discussed in Ref. [11], the contributions of the LFV couplings $\lambda^{\mu\tau}_{P,A}$ to the muon MDM, a_μ, are negative, and thus they are strongly disfavored by the current experimental data [34], which require a positive contribution to a_μ to bring the theoretical prediction closer to the experimental value. With these assumptions, we obtain the following expressions for the double differential cross sections:

$$\frac{d^2\sigma_{\mathcal{U}^0}}{dxdy}(\mu N \to \tau X) = \frac{m_N E_\mu}{8\pi\Lambda_{\mathcal{U}}^{4(d_{\mathcal{U}}-1)}}|\Delta_F(-Q^2)|^2 x q(x,Q^2) \times |\lambda^{q}_S|^2|\lambda^{\mu\tau}_S|^2 y^2, \tag{15}$$

$$\frac{d^2\sigma_{\mathcal{U}^1}}{dxdy}(\mu N \to \tau X) = \frac{m_N E_\mu}{4\pi\Lambda_{\mathcal{U}}^{4(d_{\mathcal{U}}-1)}}|\Delta_F(-Q^2)|^2 x q(x,Q^2)|\lambda^{q}_V|^2|\lambda^{\mu\tau}_V|^2 \times (1 + (1-y)^2), \tag{16}$$

with $q(x,Q^2) = u_v + d_v + 2S$. Therefore, the $\mu N \to \tau X$ cross section due to spin-0 and spin-1 unparticle exchange is

$$\sigma(\mu N \to \tau X) = \sum_{i=0,1}\int_0^1\int_0^1 \frac{d^2\sigma_{\mathcal{U}^i}}{dxdy}(\mu N \to \tau X)dxdy. \tag{17}$$

It is also useful to express the double differential cross sections of Eqs. (15) and (16) as functions of the angle of the tau lepton with respect to the beam direction and the tau energy. In terms of these variables, we have $x = Q^2/(2m_N(E_\mu - E_\tau))$ and $y = (E_\mu - E_\tau)/E_\mu$, with $Q^2 = 2E_\mu E_\tau(1 - \cos\theta)$. The transformation from the (x, y) variables to (E_τ, θ) can be written as

$$\frac{d^2\sigma_{\mathcal{U}}}{dE_\tau d\theta}(\mu N \to \tau X) = J(E_\tau, \theta)\frac{d^2\sigma_{\mathcal{U}}}{dxdy}(\mu N \to \tau X), \qquad (18)$$

where the Jacobian of the transformation from the (x, y) variables to the (E_τ, θ) variables is $J(E_\tau, \theta) = E_\tau \sin\theta/(m_N(E_\mu - E_\tau))$.

Before the numerical evaluation of Eq. (17), we need to discuss the current bounds on the fermion unparticle couplings and the unparticle scale and dimension. We will assume that the unparticle couplings to quark pairs are flavor blind, with $\lambda^q_{S,V} \simeq O(1)$, whereas for the LFV couplings $\lambda^{\mu\tau}_{S,V}$ we will consider the most stringent constraints obtained from the experimental limits on LFV tau decays and the muon MDM for values of $\Lambda_{\mathcal{U}}$ and $d_{\mathcal{U}}$ consistent with the search for monojets plus missing transverse energy at the LHC by the CMS collaboration [19].

III. NUMERICAL RESULTS AND DISCUSSION

A. Constraints on unparticle couplings

Shortly after the advent of Georgi's unparticle conjecture, bounds on the scale $\Lambda_{\mathcal{U}}$ and the dimension $d_{\mathcal{U}}$ were obtained by using the LEP data of monophoton production plus missing transverse energy [4]. More recently, the data of the search for monojet production plus missing transverse energy at the LHC were used by the CMS collaboration to constrain the parameters associated with a spin-0 unparticle [19]. It was concluded that the region $d_{\mathcal{U}} \leq 1.4$ is strongly disfavored as $\Lambda_{\mathcal{U}} \geq 10$ TeV is required to be consistent with the LHC data. On the other hand, for $d_{\mathcal{U}}$ close to 2, $\Lambda_{\mathcal{U}} \simeq 1$ TeV is still allowed. We will thus consider three illustrative sets of $(d_{\mathcal{U}}, \Lambda_{\mathcal{U}})$ values consistent with the CMS bounds, namely, (1.4, 10 TeV), (1.6, 5 TeV), and (1.9, 1 TeV). It is worth noting that the CMS bounds were obtained assuming unparticle couplings of the order of unity. So, these bounds would be weaker if couplings of smaller size were considered.

We now turn to discuss the current constraints on the LFV unparticle couplings. As stated above, for simplicity we will neglect flavor-changing neutral current unparticle couplings in the quark sector and consider that the diagonal couplings $\lambda^q_{S,V}$ are flavor blind and of the order of $O(1)$. This is in accordance, for instance, with the conclusions reached in Ref. [35], where a study of the effects of a vector unparticle on the $B \to \pi\pi$ and $B \to \pi K$ decays, combined with the constraints on $B_{d,s} - \bar{B}_{d,s}$ mixing, was presented. It was found that, for $d_{\mathcal{U}} = 1.5$, a minimum χ^2 analysis yields that the contribution of a vector unparticle can be in agreement with all the measurements of the $B \to \pi\pi$ and $B \to \pi K$ decays as long as the λ^u_V and λ^d_V couplings are of the order of $O(1)$, with both the λ^{sb}_V and λ^{db}_V couplings being of the order of 10^{-4}.

As far as the LFV unparticle couplings are concerned, they can be constrained from the experimental data of the muon MDM and the LFV decays $l_i \to l_j l_k l_k$ and $l_i \to l_j\gamma$, with $l_{i,j}$ a charged lepton. In addition, the experimental limits on the semileptonic decays $\tau \to l_i M_i$ and $\tau \to l_i M_i M_j$ [34], with $M_{i,j}$ a generic light meson, can be useful to put stringent constraints on the tau LFV couplings [36–38]. We will start by discussing the constraints obtained from the leptonic tau decay channels. By using the experimental data on the muon MDM and the $\tau \to 3\mu$ decay, the allowed region in the $\lambda^{\mu\tau}_S$ vs $\lambda^{\mu\mu}_S$ plane was obtained in Ref. [9] for several values of $d_{\mathcal{U}}$ and $\Lambda_{\mathcal{U}}$. A similar procedure was used in Ref. [11] to obtain the allowed area in the $\lambda^{\mu\tau}_V$ vs $\lambda^{\mu\mu}_V$ plane. It was also found that the loop-induced decay $l_j \to l_i\gamma$ gives a weaker constraint on such unparticle couplings. For the three sets of $(d_{\mathcal{U}}, \Lambda_{\mathcal{U}})$ values chosen above, we show in Table I the maximal allowed values of the $\lambda^{\mu\tau}_{S,V}$ couplings along with the corresponding values of the $\lambda^{\mu\mu}_{S,V}$ coupling. In general, $\lambda^{\mu\tau}_V$ is more constrained than $\lambda^{\mu\tau}_S$, but both couplings become tightly constrained when $d_{\mathcal{U}}$ gets closer to 1.4. For more details of these analyses, we refer the interested reader to the original Refs. [9,11]. We also would like to comment on the bounds obtained from the tau semileptonic decay channels. Contrary to the bounds obtained from the leptonic tau decays, in which only the couplings to lepton pairs are involved, both the couplings to lepton pairs and quark pairs enter into the semileptonic tau decay amplitudes. Under our assumptions that the nondiagonal unparticle couplings to quarks are much smaller than the diagonal ones, which we assume to be of the order of unity, the two-body decays $\tau \to \mu\pi^0$ and $\tau \to \mu\eta$ could be useful to constrain the LFV pseudoscalar $\lambda^{\mu\tau}_P$ and axial vector $\lambda^{\mu\tau}_A$ couplings, whereas the LFV vector $\lambda^{\mu\tau}_V$ coupling could be constrained via the $\tau \to \mu\rho$ and $\tau \to \mu\phi$ decays. On the other hand, the experimental limits on the three-body decays $\tau \to \mu\pi^0\pi^0$, $\tau \to \mu\eta\eta$, $\tau \to \mu\pi^-\pi^+$, etc. can translate into bounds on the scalar $\lambda^{\mu\tau}_S$ coupling. Along these lines, the authors of Ref. [39] studied the

TABLE I. 95% C.L. upper limits on the unparticle couplings $\lambda^{\mu\tau}_V$ and $\lambda^{\mu\tau}_S$, from the current bounds on the MDM and the LFV decay $\tau \to 3\mu$, for three sets of $(d_{\mathcal{U}}, \Lambda_{\mathcal{U}})$ values consistent with the bounds obtained by the CMS collaboration [19]. The corresponding values of the $\lambda^{\mu\mu}_{S,V}$ couplings are also shown.

$\Lambda_{\mathcal{U}}$ (TeV)	$d_{\mathcal{U}}$	$\lambda^{\mu\tau}_S$	$\lambda^{\mu\mu}_S$	$\lambda^{\mu\tau}_V$	$\lambda^{\mu\mu}_V$
10	1.4	4×10^{-3}	5×10^{-2}	5×10^{-4}	8×10^{-2}
5	1.6	1×10^{-2}	0.4	2×10^{-3}	0.6
1	1.9	3×10^{-2}	1.2	5×10^{-3}	4.5

constraints on LFV vector unparticle couplings from the decays $\tau \to \mu V^0$ ($V^0 = \rho, \omega, \phi$). However, it was concluded that the resulting constraints turn out to be weaker than the constraints obtained from the muon MDM and the leptonic tau decays for $\Lambda_{\mathcal{U}} = 1$ TeV, $1.6 \leq d_{\mathcal{U}} \leq 2$ and values of the unparticle couplings to quark pairs in the interval 0.1–1 [39]. We will thus consider the restrictions of Table I in the following analysis.

In summary, to illustrate the behavior of the $\mu N \to \tau X$ cross section, we will consider the maximal allowed values of the $\lambda^{\mu\tau}_{S,V}$ couplings consistent with the current bounds on the muon MDM and the LFV decay $\tau \to 3\mu$, for three sets of $(d_{\mathcal{U}}, \Lambda_{\mathcal{U}})$ values consistent with the bounds obtained by the CMS collaboration.

B. Unparticle contribution to the $\mu P \to \tau X$ cross section

We now turn to the numerical analysis. We will consider that the target is a proton and use the CTEQ6m parton distribution functions [40]. We show the spin-0 and spin-1 unparticle contributions to the $\mu P \to \tau X$ cross section in Fig. 2 as a function of the muon energy and for three sets of $(d_{\mathcal{U}}, \Lambda_{\mathcal{U}})$ values. For each such set, we used the corresponding maximal allowed values of $\lambda^{\mu\tau}_S$ and $\lambda^{\mu\tau}_V$ shown in Table I. In Fig. 2 we present two plots in which we consider a different cut in the momentum transfer: in the left plot we take $Q > 2$ GeV, whereas in the right plot we use $Q > 1.6$ GeV. Since $\lambda^q_{S,V} \simeq O(1)$ was assumed for all the quarks, it is worth noting that if this coupling was decreased by one order of magnitude, the cross section would decrease by two orders of magnitude. For comparison purposes, we have also included in these plots the contribution to the $\mu P \to \tau X$ cross section from the dimension-six effective scalar-mediated four-fermion LFV vertex $\bar{\tau}\mu\bar{q}q$, which was already studied by the authors of Ref. [32], who focused on the contribution of Higgs exchange in the context of the MSSM. We note that our results agree with those presented in Ref. [32], which serves as a cross-check for our calculation.

It is interesting that the $\mu P \to \tau X$ cross section is larger when $d_{\mathcal{U}} = 1.4$ and smaller when $d_{\mathcal{U}}$ approaches 2, which contrasts with the size of the values assumed for the LFV unparticle coupling $\lambda^{\mu\tau}_{S,V}$ and the unparticle scale $\Lambda_{\mathcal{U}}$; according to the aforementioned bounds, when $d_{\mathcal{U}} = 1.4$, $\lambda^{\mu\tau}_{S,V}$ is smaller and $\Lambda_{\mathcal{U}}$ is larger, but when $d_{\mathcal{U}} = 1.9$, $\lambda^{\mu\tau}_{S,V}$ is larger and $\Lambda_{\mathcal{U}}$ is smaller. The results observed in Fig. 2 stem from the behavior of the unparticle propagator [Eq. (2)]: the unparticle contribution behaves as that of a massless particle as $d_{\mathcal{U}} \to 1$, but it approaches the contribution of a four-fermion contact vertex when $d_{\mathcal{U}} \to 2$. We also note that the spin-0 unparticle contributions are larger by more than one order of magnitude than the spin-1 unparticle contributions, which is a result of the values used for the $\lambda^{\mu\tau}_V$ and $\lambda^{\mu\tau}_S$ couplings. This situation is also observed in the case of the scalar-mediated and the vector-mediated contributions studied in Refs. [31,32]. Finally, although both the spin-0 and the spin-1 unparticle contributions increase steadily with E_μ, such increase is not as dramatic as it does occur in the case of the MSSM contribution.

Figure 2 also shows the sensitivity of the $\mu P \to \tau X$ cross section to the cut in the momentum transfer. This is also a reflect of the infrared behavior of the unparticle propagator. Even if the cut $Q > 2$ GeV is imposed, for a wide range of E_μ values, the unparticle contributions can be larger than the MSSM contribution, though the latter increases suddenly around $E_\mu = 50$ GeV and continues to increase steadily. As explained in Ref. [32], such a dramatic increase is due to the contribution of the sea b quark,

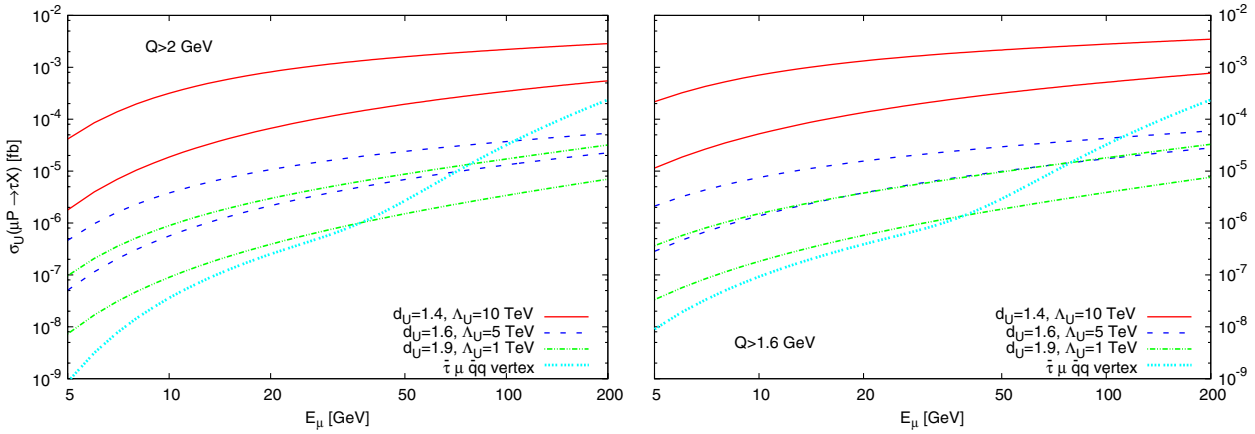

FIG. 2 (color online). $\mu P \to \tau X$ cross section due to LFV unparticle couplings for three sets of $(d_{\mathcal{U}}, \Lambda_{\mathcal{U}})$ values. For the LFV coupling $\lambda^{\mu\tau}_{S,V}$ we used the values shown in Table I, whereas $\lambda^q_{V,S} \simeq O(1)$ was assumed for all the unparticle-quark couplings. A cut of $Q > 2$ (1.6) GeV was used in the left (right) plot. For each line style, the upper lines correspond to the contribution from a spin-0 unparticle, whereas the lower lines represent the contribution from a spin-1 unparticle. For comparison purpose, we also show the contribution from a dimension-six effective four-fermion LFV vertex $\bar{\tau}\mu\bar{q}q$, considering the coupling values used in Ref. [32] for the contribution of Higgs exchange in the MSSM.

which is enhanced by a factor of $(m_b/m_s)^2$ with respect to that of the sea s quark. On the other hand, the unparticle contributions are considerably smaller than those obtained in Ref. [31] for the calculation of the quasielastic process $\mu N \to \tau N$ using the four-fermion LFV scalar coupling. However, in that analysis, a value of $4\pi/\Lambda^2$, with $\Lambda = 1$ TeV, was used for the associated coupling constant, whereas we are considering strong bounds on the LFV unparticle coupling constants.

C. Angular and energy distributions of the emitted tau lepton

We now would like to discuss the behavior of the angular and energy distributions of the emitted tau lepton for our DIS process, which could be a useful tool to disentangle the unparticle contributions from other class of effects. For this purpose, in Fig. 3 we show the contour lines of the spin-0 unparticle-mediated double differential cross section $\frac{d^2\sigma_{\mathcal{U}}}{dE_\tau d\theta}(\mu P \to \tau X)$ for the same sets of parameter values of Table I and two values of the muon energy. The analogous plots for the spin-1 unparticle-mediated contribution show a similar behavior, and we refrain from presenting them here. It is worth noting that the cut $Q > 2$ GeV was used in these plots, which explains the white area closer to $\theta = 0$. In fact, in this area the double differential cross section could reach its higher values depending on the $d_{\mathcal{U}}$ value, as will be discussed below. Also, our calculation automatically excludes the kinematically forbidden region, which appears as the unshaded area in the top right corner of each plot. Due to the

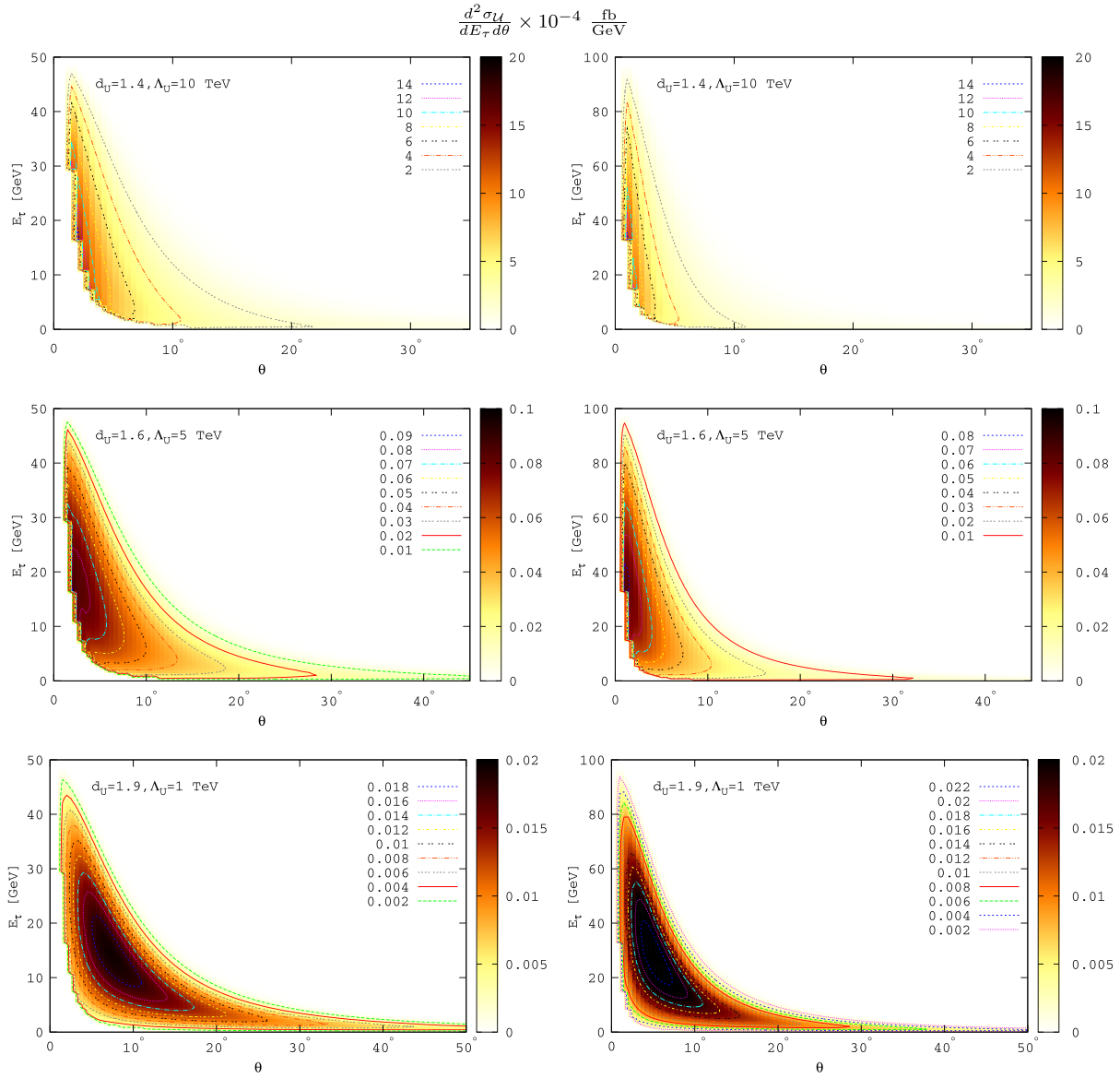

FIG. 3 (color online). Contour plots for the spin-0 unparticle-mediated double differential cross section $\frac{d^2\sigma}{dE_\tau d\theta}(\mu P \to \tau X)$ for $E_\mu = 50$ GeV (left plots) and $E_\mu = 100$ GeV (right plots) for the parameters of Table I. The cut $Q > 2$ GeV is imposed.

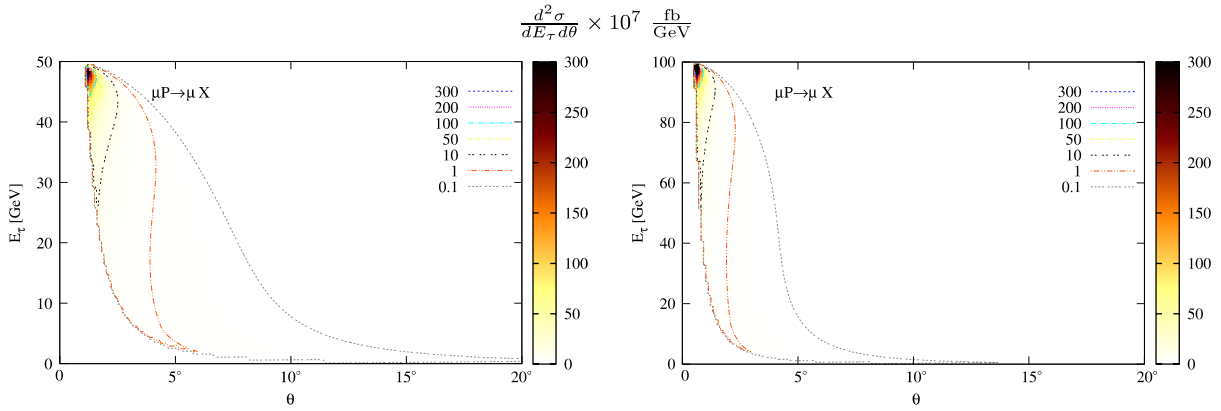

FIG. 4 (color online). Contour plots for the double differential cross section $\frac{d^2\sigma}{dE_\tau d\theta}(\mu P \to \mu X)$ for $E_\mu = 50$ GeV (left plot) and $E_\mu = 100$ GeV (right plot). The cut $Q > 2$ GeV is imposed.

infrared behavior of the unparticle propagator [Eq. (2)], it is expected that the tau lepton would be emitted preferentially along the forward direction of the beam when $d_{\mathcal{U}}$ is close to 1. This is shown in Fig. 3, where the darker area on the contour plots, which is associated with the higher values of the double differential cross section, spreads around $\theta = 0$, i.e., the higher values of the double differential cross section are reached around $\theta = 0$. We can see that the darker area is relatively wider at low tau energies, but it shrinks considerably as the tau energy increases. It means that, in this situation, a low-energy tau would be emitted at a larger angle than a high-energy tau. On the other hand, the situation is rather different when $d_{\mathcal{U}}$ approaches 2, when the infrared behavior of the unparticle propagator is less pronounced. We thus observe that, when $d_{\mathcal{U}} = 1.9$, the darker area in the contour plot shrinks considerably and also shifts rightward and upward. In this case the preferred emission angle of the tau lepton is no longer located close to the forward beam direction but at a slightly larger angle whose value increases as the muon energy increases. Again, a low-energy tau would tend to be emitted at a larger angle than an energetic tau.

In conclusion, when $d_{\mathcal{U}} = 1.4$ we expect that the $\mu P \to \tau X$ double differential cross section behaves similarly to that of photon-mediated $\mu P \to \mu X$ DIS, which in fact would be the main source of background for our process. On the other hand, when $d_{\mathcal{U}} = 1.9$ the behavior of the $\mu P \to \tau X$ double differential cross section would resemble that of the Higgs-mediated one. It is interesting to contrast the behavior of all these kinds of contributions. We thus show in Fig. 4 the photon-mediated $\mu P \to \mu X$ double differential cross section, whereas the Higgs-mediated $\mu P \to \tau X$ double differential cross section is shown in Fig. 5. In the former case (Fig. 4) we observe that the double differential cross section is strongly peaked at a low angle and a high energy: in this scenario, the signature of the process would be an energetic muon emitted close to the forward beam direction. Therefore, the photon-mediated $\mu P \to \mu X$ is highly sensitive to a cut in the transfer momentum Q. As far as the Higgs-mediated double differential cross section is concerned, we observe in Fig. 5 that the tau lepton would be emitted preferentially with a low energy (below one half the muon energy) and at an angle considerably larger than that of the forward beam

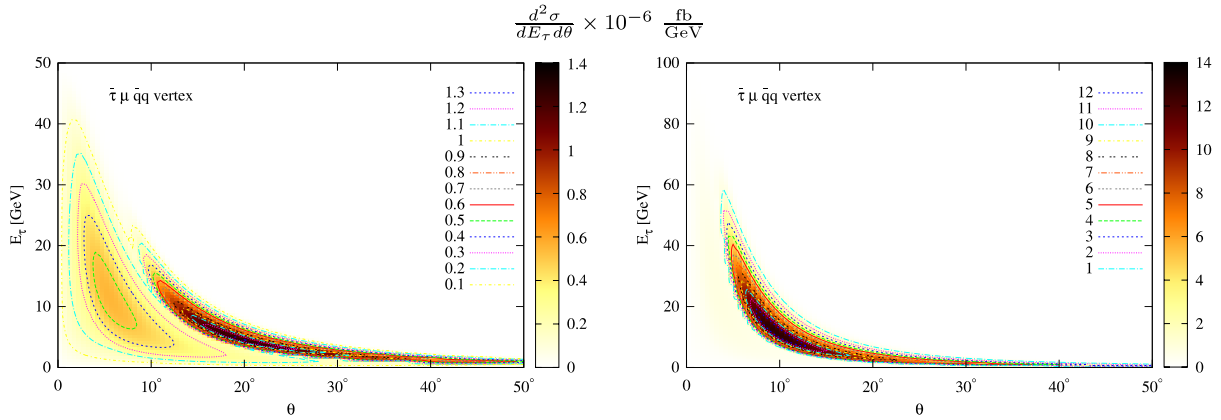

FIG. 5 (color online). Contour plots for the Higgs-mediated double differential cross section $\frac{d^2\sigma}{dE_\tau d\theta}(\mu P \to \tau X)$ for $E_\mu = 50$ GeV (left plot) and $E_\mu = 100$ GeV (right plot). We used the same coupling values used in Ref. [32]. No cut is imposed.

direction: around 20° for $E_\tau = 50$ GeV and around 10° for $E_\tau = 100$ GeV. It is also interesting to note that the Higgs-mediated double differential cross section shows two peaks, though the higher peak appears at a larger angle.

More details of the behavior of the angular distribution of the tau lepton can be extracted from Fig. 6, where, for the same parameter values used previously, we have plotted the unparticle-mediated $\frac{d^2\sigma_\mathcal{U}}{dE_\tau d\theta}(\mu P \to \tau X)$ double differential cross section as a function of θ, for several fixed values of E_τ. We show plots for two values of E_μ, namely, 50 GeV and 100 GeV. We can distinguish two cases: when $d_\mathcal{U}$ is close to 1 and when $d_\mathcal{U}$ is close to 2. In the first case, when $d_\mathcal{U} = 1.4$, we can observe that the tau lepton is emitted preferentially at angles smaller than 35°, but the double differential cross section is considerably larger around $\theta = 0$, which means that the preferred emission angle of the tau lepton is $\theta = 0$. As its energy increases, the tau lepton would tend to be emitted closer to the forward direction of the beam.

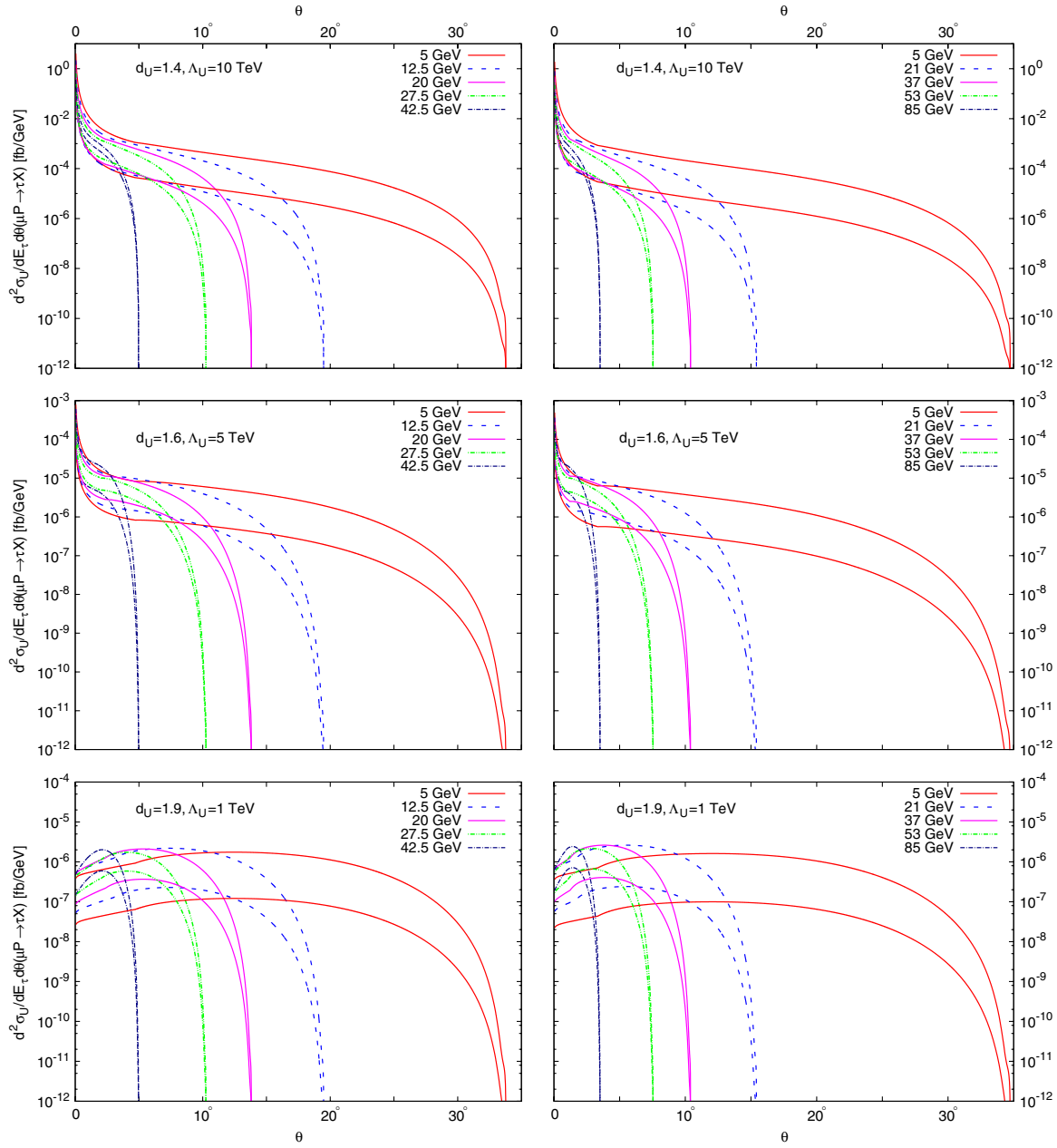

FIG. 6 (color online). Unparticle contribution to the double differential cross section $\frac{d^2\sigma}{dE_\tau d\theta}(\mu P \to \tau X)$ as a function of the tau emission angle θ for several values of the tau energy E_τ and two values of E_μ: 50 GeV (left plots) and 100 GeV (right plots). We considered the three sets of parameter values of Table I. For each line style, the upper lines correspond to the spin-0 unparticle contribution, whereas the lower lines represent the spin-1 unparticle contribution.

For instance, a tau lepton with about 90% the beam energy would be emitted preferentially at $\theta \leq 5°$, whereas a tau lepton with an energy about 10% the beam energy would be emitted mainly at $\theta \leq 35°$. The situation changes drastically when $d_{\mathcal{U}}$ is close to 2, namely, $d_{\mathcal{U}} = 1.9$, in which case the tau lepton is emitted preferentially at large angles, although the preferred angle gets closer to the forward direction of the beam if the tau lepton energy is high. In this scenario, when E_τ is about 10% of the beam energy, the preferred emission angle of the tau lepton is around 20°, whereas it is around 5° when E_τ is about 90% of the beam energy.

The effects discussed above are also evident when we analyze the energy distribution of the tau lepton. This is shown in Fig. 7, where this time we have plotted the double differential cross section as a function of E_τ for several values of the emission angle θ and two values of E_μ. We have used the same set of parameter values used in the previous figures. We observe that the curves corresponding to increasing values of θ are shifted downward and

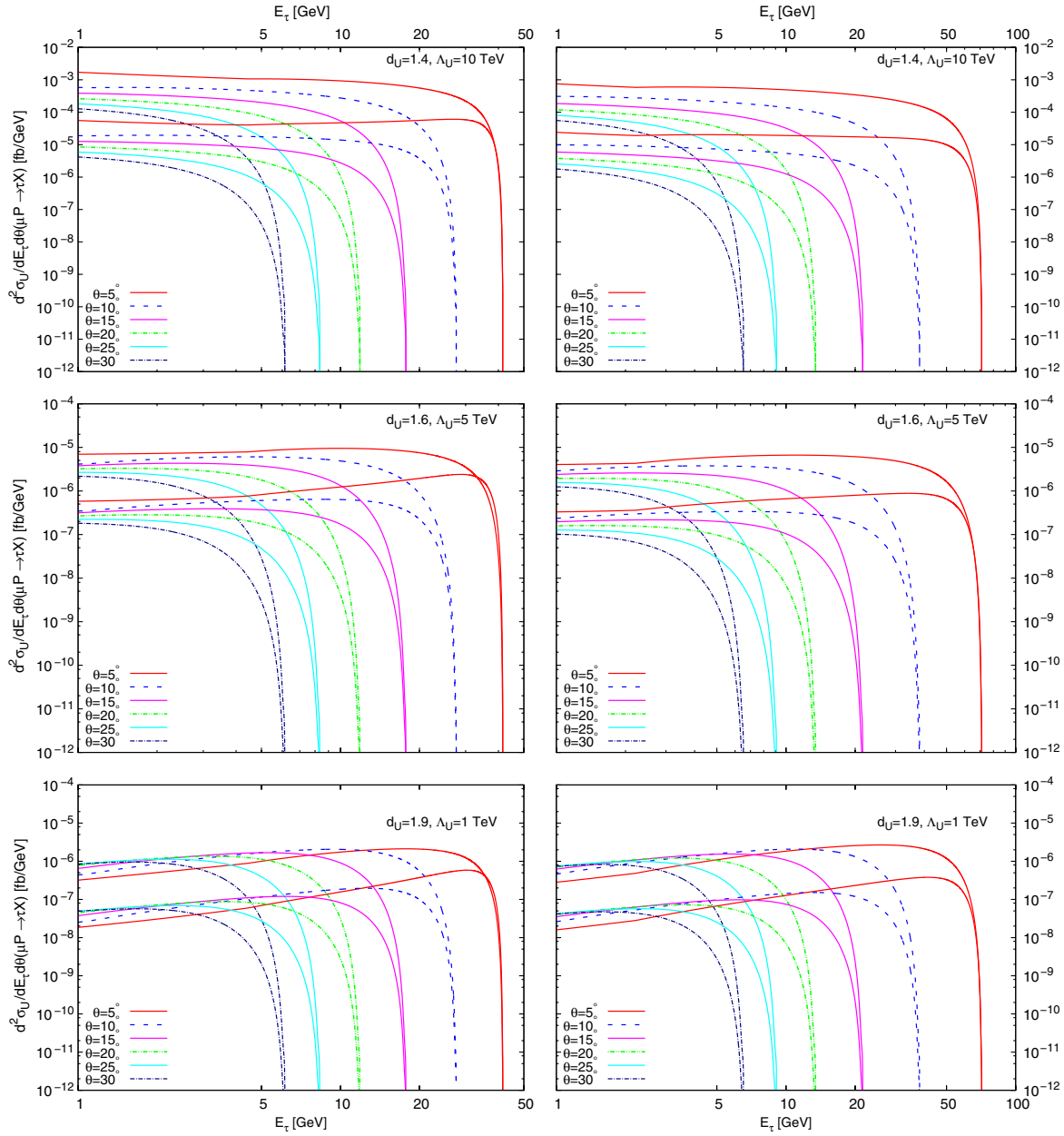

FIG. 7 (color online). Unparticle contribution to the double differential cross section $\frac{d^2\sigma}{dE_\tau d\theta}(\mu P \to \tau X)$ as a function of the tau energy E_τ for several values of the emission angle θ and two values of E_μ: 50 GeV (left plots) and 100 GeV (right plots). We considered the three sets or parameter values of Table I. For each line style, the upper lines correspond to the spin-0 unparticle contribution, whereas the lower lines represent the spin-1 unparticle contribution.

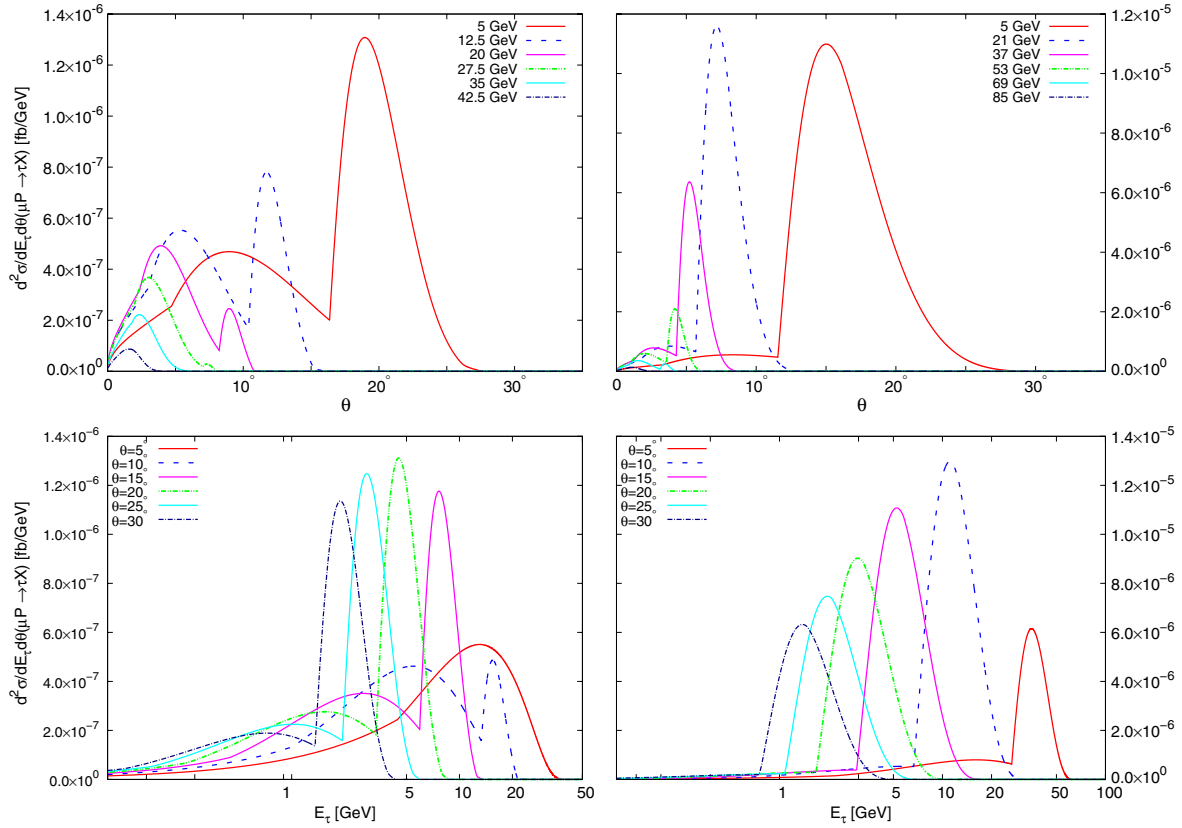

FIG. 8 (color online). Contribution to the double differential cross section $\frac{d^2\sigma}{dE_\tau d\theta}(\mu P \to \tau X)$ from a dimension-six effective four-fermion LFV vertex $\bar{\tau}\mu\bar{q}q$, considering the coupling values used in Ref. [32]. The upper plots show the dependence on the tau scattering angle θ for several values of the tau energy E_τ, whereas the lower plots show the dependence on the tau energy for several values of the tau scattering angle. Two values of the muon energy are used: $E_\mu = 50$ GeV (left plots) and $E_\mu = 100$ GeV (right plots).

leftward. The area under each curve shrinks considerably as θ increases, which means that the bulk of the contribution to the cross section arises mainly in the region of small angles, though this situation changes slightly as $d_{\mathcal{U}} \to 2$. Although the behavior of the differential cross section could be expected to be similar to that induced by a massless intermediary particle, the nature of the unparticle propagator makes this effect very distinctive as it is tuned by the value of the dimension $d_{\mathcal{U}}$. We note, however, that all the analysis we have done so far shows that there is little difference between the contributions to the $\mu P \to \tau X$ process from a spin-0 unparticle and from a spin-1 unparticle, so unparticle contributions would be hard to disentangle using this kind of analysis.

Finally, we would like to contrast the behavior of the angular and energy distributions of the unparticle-mediated contribution to the $\mu P \to \tau X$ process with that of the contribution from Higgs exchange [32]. For comparison purposes, we have made analogous plots to the ones shown in Figs. 6 and 7 using the same parameter values as in Ref. [32]. The results are presented in Fig. 8, where we show the behavior of the scalar contribution to the $\mu P \to \tau X$ double differential cross section as a function of θ (upper plots) and E_τ (lower plots), for two values of E_μ. In this case a low-energy tau lepton is emitted preferentially at a relatively large angle, whereas a high-energy tau lepton is emitted closer to the forward direction of the beam. When the muon energy increases, the preferred emission angle decreases. For instance, for $E_\mu = 50$ GeV the largest peak in the double differential cross section is around $\theta = 20°$, but for $E_\mu = 100$ GeV the largest peak is around $\theta = 10°$.

D. Background

A beam with intensity of 10^{20} muons per year is expected at a neutrino factory, with the muon energy in the range of a few dozens of GeVs [33]. It has been estimated [31] that, a cross section for the muon-nucleon collision of the order of 1 fb would yield a probability of interactions per meter of about $6 \times 10^{-14}\rho$ in a meter of target as long as there is little ionization loss. Here ρ is the density of the target expressed in g/cm^3. Assuming 10^{20} muons per year on a 10^2 g/cm^2 target mass would yield about $10^6 \mu N \to \tau X$ events annually. The unparticle contributions to the $\mu P \to \tau X$ cross section are smaller than 1 fb, but in a promising scenario we would have a cross section of the order of 10^{-4}–10^{-3} fb, which would yield

about 10^2–10^3 $\mu P \to \tau X$ events annually, though there would be some enhancement if the target is an atom nucleus. The main issue for the detection of the signal of this reaction will be the identification of the tau lepton from its decay products. If the leptonic decay channel $\tau \to \mu \bar{\nu}_\mu \nu_\tau$ is considered, the most dangerous background is expected to arise from the lepton flavor-conserving reaction $\mu P \to \mu X$, which would proceed mainly via QED. For this reaction the muon would also emerge dominantly along the beam forward direction, though its energy distribution would be rather different than that of the muon arising from the tau decay. A detailed discussion about reducing this background can be found in Ref. [30]. Other possibilities for detection of the tau lepton has been examined in Ref. [32], such as considering the hadronic tau decay $\tau \to \pi \nu_\tau$. In this case, the main problem arises from the misidentification of the pion with the muon arising from $\mu P \to \mu X$. A more detailed Monte Carlo analysis would be required to make further conclusions.

IV. CONCLUSIONS

We have studied $\mu - \tau$ conversion through the $\mu P \to \tau X$ process mediated by spin-0 and spin-1 unparticles. For the model parameters, we used the most recent constraints on the LFV unparticle couplings $\lambda_{S,V}^{\mu\tau}$ from the muon MDM and the tau decay $\tau \to 3\mu$. These values are also consistent with the most recent bounds on the unparticle scale $\Lambda_{\mathcal{U}}$ and the dimension $d_{\mathcal{U}}$ from the data of the search for monojets plus missing transverse energy at the LHC by the CMS collaboration. In a promising scenario, the resulting cross section can be of the order of 10^{-3}–10^{-2} fb for $d_{\mathcal{U}} = 1.4$ and $\Lambda_{\mathcal{U}} = 10$ TeV. Due to the infrared nature of the unparticle propagator, the angular distribution of the emitted tau lepton is rather different than that observed in the case of other contributions: in the unparticle mediated process, the tau lepton is emitted mainly along the forward beam direction. For a beam with intensity of 10^{20} 50 GeV muons per year on a target nucleon of 10^2 gr/cm^2 mass, there would be about 10^2–10^3 $\mu P \to \tau X$ events annually, which would open up the possibility for a more detailed Monte Carlo analysis. The potential issues with the signal detection would be the identification of the emitted tau lepton through its decay products. Two promising tau decay channels are the leptonic decay $\tau \to \mu \bar{\nu}_\mu \nu_\tau$ and the hadronic decay $\tau \to \pi \mu \bar{\nu}_\tau$. In any case, the main background is expected to arise from the lepton flavor conserving $\mu P \to \mu X$ process, whose signal could mimic that of the muon or the pion arising from the tau decay channels.

ACKNOWLEDGMENTS

We would like to thank SNI and Conacyt (México) for financial support. G. T. V. would like to thank VIEP-BUAP for support.

[1] H. Georgi, Phys. Rev. Lett. **98**, 221601 (2007).
[2] H. Georgi, Phys. Lett. B **650**, 275 (2007).
[3] T. Banks and A. Zaks, Nucl. Phys. **B196**, 189 (1982).
[4] K. Cheung, W. Y. Keung, and T. C. Yuan, Phys. Rev. D **76**, 055003 (2007).
[5] K. Cheung, W. Y. Keung, and T. C. Yuan, Phys. Rev. Lett. **99**, 051803 (2007).
[6] P. Mathews and V. Ravindran, Phys. Lett. B **657**, 198 (2007).
[7] M. C. Kumar, P. Mathews, V. Ravindran, and A. Tripathi, Phys. Rev. D **77**, 055013 (2008).
[8] T. G. Rizzo, Phys. Lett. B **665**, 361 (2008).
[9] A. Hektor, Y. Kajiyama, and K. Kannike, Phys. Rev. D **78**, 053008 (2008).
[10] E. O. Iltan, Int. J. Mod. Phys. A **24**, 2729 (2009).
[11] A. Moyotl, A. Rosado, and G. Tavares-Velasco, Phys. Rev. D **84**, 073010 (2011).
[12] G. J. Ding and M. L. Yan, Phys. Rev. D **77**, 014005 (2008).
[13] R. Martinez, M. A. Perez, and O. A. Sampayo, Int. J. Mod. Phys. A **25**, 1061 (2010).
[14] Y. Liao, Phys. Rev. D **76**, 056006 (2007).
[15] M. Luo and G. Zhu, Phys. Lett. B **659**, 341 (2008).
[16] C. H. Chen and C. Q. Geng, Phys. Rev. D **76**, 115003 (2007).
[17] C. S. Huang and X. H. Wu, Phys. Rev. D **77**, 075014 (2008).
[18] J. Barranco, A. Bolaños, O. G. Miranda, C. A. Moura, and T. I. Rashba, Phys. Rev. D **79**, 073011 (2009).
[19] S. Chatrchyan *et al.* (CMS Collaboration), Phys. Rev. Lett. **107**, 201804 (2011).
[20] H. Davoudiasl, Phys. Rev. Lett. **99**, 141301 (2007).
[21] S. Hannestad, G. Raffelt, and Y. Y. Y. Wong, Phys. Rev. D **76**, 121701 (2007).
[22] P. K. Das, Phys. Rev. D **76**, 123012 (2007).
[23] A. Freitas and D. Wyler, J. High Energy Phys. 12 (2007) 033.
[24] J. Adam *et al.* (MEG Collaboration), Phys. Rev. Lett. **107**, 171801 (2011).
[25] U. Bellgardt *et al.* (SINDRUM Collaboration), Nucl. Phys. **B299**, 1 (1988).
[26] J. Kaulard *et al.* (SINDRUM II Collaboration), Phys. Lett. B **422**, 334 (1998).
[27] B. Aubert *et al.* (*BABAR* Collaboration), Phys. Rev. Lett. **104**, 021802 (2010).
[28] B. Aubert *et al.* (*BABAR* Collaboration), Phys. Rev. Lett. **99**, 251803 (2007).
[29] Y. Miyazaki *et al.* (Belle Collaboration), Phys. Lett. B **660**, 154 (2008).

[30] S. N. Gninenko, M. M. Kirsanov, N. V. Krasnikov, and V. A. Matveev, Mod. Phys. Lett. A **17**, 1407 (2002).
[31] M. Sher and I. Turan, Phys. Rev. D **69**, 017302 (2004).
[32] S. Kanemura, Y. Kuno, M. Kuze, and T. Ota, Phys. Lett. B **607**, 165 (2005).
[33] S. Choubey *et al.* (IDS-NF Collaboration), arXiv:1112.2853.
[34] J. Beringer *et al.* (Particle Data Group Collaboration), Phys. Rev. D **86**, 010001 (2012).
[35] C.-H. Chen, C. S. Kim, and Y. W. Yoon, Phys. Lett. B **671**, 250 (2009).
[36] D. Black, T. Han, H.-J. He, and M. Sher, Phys. Rev. D **66**, 053002 (2002).
[37] A. Brignole and A. Rossi, Nucl. Phys. **B701**, 3 (2004).
[38] M. Sher, Phys. Rev. D **66**, 057301 (2002); see also T. Fukuyama, A. Ilakovac, and T. Kikuchi, Eur. Phys. J. C **56**, 125 (2008).
[39] Z.-H. Li, Y. Li, and H.-X. Xu, Phys. Lett. B **677**, 150 (2009).
[40] J. Pumplin, D. R. Stump, J. Huston, H. L. Lai, P. M. Nadolsky, and W. K. Tung, J. High Energy Phys. 07 (2002) 012.